NUMERICAL INVESTIGATION OF THE SEISMIC RESPONSE OF SQUARE HSS BRACES WITH INTENTIONAL ECCENTRICITY

A. González Ureña(1), R. Tremblay(2), C. A. Rogers(3)

(1) Ph.D. candidate, Department of Civil Engineering and Applied Mechanics, McGill University, andres.gonzalezurena@mcgill.ca
(2) Professor, Department of Civil, Geological and Mining Engineering, Polytechnique Montréal, robert.tremblay@polymtl.ca
(3) Professor, Department of Civil Engineering and Applied Mechanics, McGill University, colin.rogers@mcgill.ca

Abstract

Concentrically Braced Frames (CBFs) comprising Hollow Structural Section (HSS) bracing members possess high stiffness and are susceptible to premature local buckling at the plastic hinge region, leading to low-cycle fatigue induced fracture. Intentionally offsetting the axis of otherwise conventional steel braces with respect to the working points has been proposed to overcome these shortcomings. Braces with Intentional Eccentricity (BIEs), the novel type of brace proposed by researchers in Japan, are subject to bending moment in addition to axial force under seismic action and, as such, inherently possess lower axial stiffness than Conventional Concentric Braces (CCBs). Their pre- and post-yielding stiffness can be adjusted by varying the eccentricity, allowing for better control of the structure's dynamic response to ground motion excitations. A single experimental study has been performed on BIEs, with results indicating that, in comparison with CCBs, local buckling and fracture occurred in BIEs at significantly higher drift ratios due to the strain demand being more evenly distributed along the brace length.

A numerical investigation has been undertaken to verify the generalisation of this behaviour to square HSS BIEs with different global and local slenderness ratios and to shed light on the range of imposed axial deformation these braces are able to sustain safely, as function of the eccentricity and their global and local slenderness. The investigation consists of a parametric study of finite element models of BIEs considering global slenderness ratios (L/r) ranging from 50 to 200, local slenderness ratios (b/t) between 4 and 36 and eccentricity ratios (e/H) from 0 (i.e. that of a CCB) to 2. Based on cost-effectiveness from a constructive point of view, and since the study is planned to be continued by the physical testing of full-scale BIE specimens, the BIE models were designed considering that the eccentricity is introduced by an assembly consisting of welded side plates linking the bracing members to the end connections. It was observed that the introduction of the eccentricity does delay, in terms of axial displacement, or imposed drift ratio, the onset of local buckling and thus, presumably, the fracturing of the brace. The article presents the numerical study and discusses the results and their implications for the design of Frames with Intentionally Eccentric Braces (FIEBs). An equation for predicting the deformation capacity of BIEs is proposed. Recommendations regarding the equivalent damping properties of BIEs for their use in the context of a Displacement-Based Design approach are also provided.

Keywords: steel braced frames; braces with intentional eccentricity; frames with intentionally eccentric braces; numerical investigation; earthquake-resistant design

1. Introduction

Concentrically Braced Frames (CBFs) constitute an often-favoured choice for the Seismic-Force-Resisting System (SFRS) of low- to mid-rise buildings in earthquake-prone regions due to their cost-effectiveness. In these, Hollow Structural Sections (HSSs) are frequently selected as the bracing members, owing to their efficiency in compression over other section shapes, and to their aesthetic appeal. However, CBFs with HSS bracing members bear significant drawbacks that limit their advantages. Primarily, it has been demonstrated in research [1, 2] that HSSs are susceptible to low-cycle fatigue fracturing as a result from the large concentration of strains in the mid-length plastic hinge after the onset of local buckling. Additionally, as Conventional Concentric Braces (CCBs) possess negligible post-yielding stiffness, large deformation demands, potentially triggering instability, are a concern. Finally, as an implication of their inherently high stiffness, CBFs are confined to low fundamental vibration periods, and therefore to larger spectral acceleration demands than in other, more flexible, systems, which, in combination with the overstrength ensuing from the difference between the tensile and compressive capacities of the braces, entails high capacity-based design forces for the non-dissipating members of the SFRS and its foundations, that reverberate in the cost of the structure.

Recently, the concept of Braces with Intentional Eccentricity (BIEs) has been proposed by Skalomenos et al. [3] as an alternative to CCBs that overcomes the deficiencies listed above. Simply put, a BIE is an otherwise conventional bracing member, with its longitudinal axis offset perpendicularly with respect to the working points, or braced frame diagonal. Being subject to bending moment in addition to axial force under earthquake loading, BIEs are substantially more flexible than CCBs and exhibit a distinct force-deformation response that sets them apart from CCBs and other traditional dissipative elements. Under monotonic tension, BIEs present a pseudo tri-linear response, with a significant post-yielding stiffness that depends on the prescribed eccentricity, while in compression, they show a steady flexural behaviour, devoid of salient peaks corresponding to buckling. In their study, Skalomenos et al. performed physical tests of reduced scale BIE specimens under cyclic loading, and their results confirmed the behaviour described above. They also showed that, in comparison with CCBs, BIEs benefit from a longer fracture life, in terms of allowable imposed drift ratio under cyclic loading, as due to the eccentricity, the strain demand is more evenly distributed along the brace length, thus delaying the onset of local buckling at the central plastic hinge region.

Considering their particular force-deformation behaviour, the authors of this article advocate a Displacement-Based Design based procedure as being appropriate in the design of Frames with Intentionally Eccentric Braces (FIEBs). This is expanded upon in a paper companion to the present one [4]. In the proposed design procedure, the predicted fracture life of BIEs and the equivalent damping ratio associated to them, constitute essential inputs: the former defines the maximum target displacements that the designer can specify, and on the latter depends the scaling factor to apply to the design displacement spectrum. In this paper, results from a numerical parametric study are presented aiming to shed light on the range of imposed cyclic axial deformation, or storey drifts, that square HSS BIEs can safely sustain before the onset of local buckling, as a function of the prescribed eccentricity and the global and local slenderness ratios. Information is also provided regarding the energy dissipation and equivalent damping properties of BIEs.

2. Properties of BIEs

The components of a nonspecific BIE are presented in Fig. 1. The eccentricity, e, is defined as the parallel offset between the bracing member's longitudinal axis and the line of action of the forces transmitted by the frame, or working points' axis. The eccentricity is introduced by the *eccentering* assemblies, which in general can be any arrangement of plates designed to accommodate the eccentricity, while linking rigidly the bracing member to its end connections and subsequently to the frame members. In the figure, the connections are shown as pins, however, in a realistic scenario, a free rotation condition of the BIE's end would be approximated by detailing the connection such that it yields in flexure for low levels of force, as is done often for CCBs. The force-deformation behaviour of a BIE depends on the bracing member's cross section and its material, the prescribed eccentricity, e, the hinge-to-hinge length, L, and the *eccentering* assemblies' length, L_{ea}.

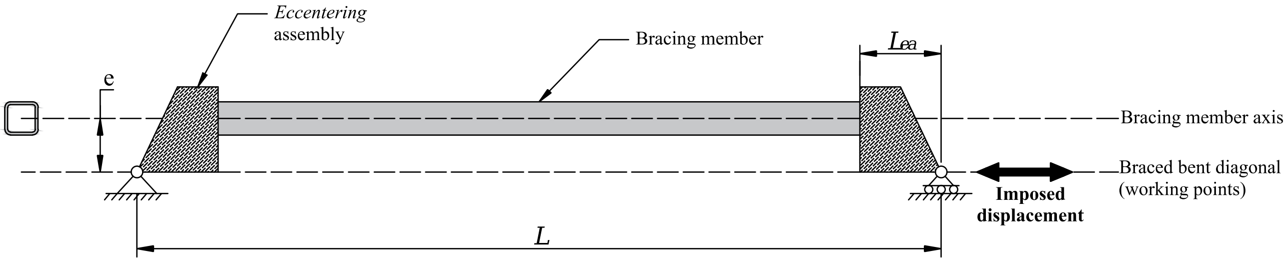

Fig. 1 – Schematic drawing of a general BIE and its components

The typical force-deformation behaviour of BIEs under monotonic tensile (a) and compressive (b) loading is presented in Fig. 2. In contrast with CCBs, whose behaviour in tension is close to elastic-perfectly plastic, the BIEs show a response in tension that can be idealised as tri-linear. For low levels of tensile load or imposed displacement, the BIE responds elastically in combined flexure and axial load and the brace bends toward the working points axis. When the outermost fiber in tension attains the yielding stress, the BIE is said to have reached its "first yield point" (T_Y, δ_Y) and the force-deformation curve transitions from the initial, or elastic, regime into the secondary, or post-yielding regime, which presents a markedly lower, although significant, stiffness. As the displacement increases, the effective eccentricity decreases, entailing a gradual increment of the stiffness while the yielding of the cross-section progresses. As the full cross-section yields, the BIE attains its "ultimate yield point" (T_U, δ_U), whose load level is the same as the yield tensile strength of a CCB of the same section, but at a significantly greater displacement. The force-deformation of BIEs in tension can thus be approximated by a tri-linear model: a starting segment with initial, or elastic, stiffness, K_i, that extends to the first yield point, followed by a second segment with secondary, or post-yielding stiffness, K_s, until the ultimate yield point is attained, and a third, fully yielded, segment with negligible stiffness. In compression, BIEs present a smooth flexural response. As the compressive loading increases, the brace bends away from the axis connecting its working points, and hence its stiffness reduces progressively. Opposed to the characteristic response of CCBs in compression, which presents a prominent peak corresponding to overall buckling, the BIEs transition seamlessly from the elastic to the post-buckling regimes. It is proposed that the response of BIEs in compression be approximated with an elastic-perfectly plastic model, with initial stiffness K_i, and with maximum compressive load, C', calculated as the elastic limit state of a column under eccentric axial load, as proposed in [3].

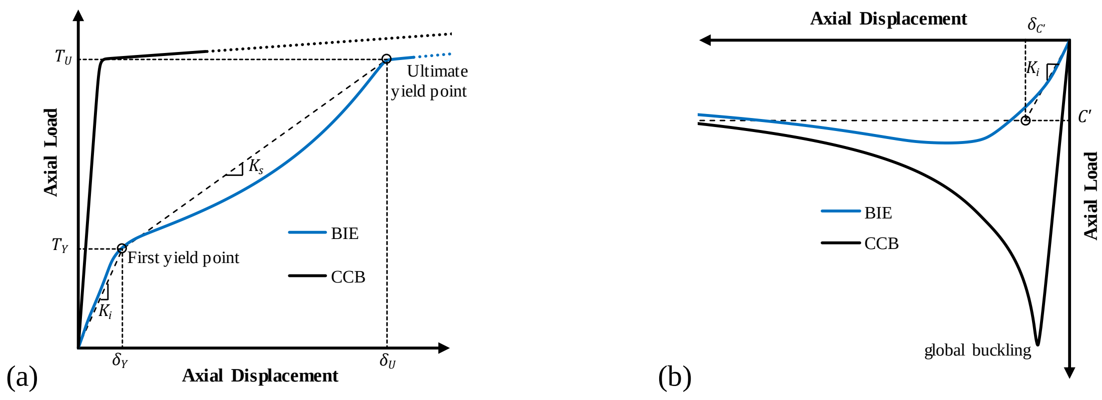

Fig. 2 – Idealised force-deformation behaviour of BIEs and CCBs: tension, (a), and compression, (b)

The influence of the eccentricity on the values of K_i, K_s, and T_Y can be observed in Fig. 3, which was constructed using results of fiber models of 178×178×16 HSS BIEs in OpenSees [5]. In these models, all parameters were kept constant, except for the eccentricity to showcase, its effects on the tensile response of BIEs. The overall length, L, was 5408 mm and the *eccentering* assemblies were represented by rigid links with length, L_{ea}, of 360 mm. The end connections were modelled as rectangular plates with thickness of 38.1 mm and width of 360 mm, and a free length of 77 mm intended to yield in flexure under low levels of force, thus approximating the desired pin-like behaviour. The yield stress was taken as 345 MPa both for the plates and the HSS.

The particularities of the BIEs' force-deformation response translate also to cyclic loading, as shown in Fig. 4, which compares the force-deformation hysteresis plots of CCBs and BIEs of the same section, under cyclic load with increasing displacement amplitude, obtained from OpenSees analyses based on dimensions consistent with a 6 m by 4 m braced bay. In spite of being capable of opposing, in net terms, less resistance and dissipating less energy than the CCBs, the BIE's response shows promising features such as the lack of peaks due to buckling, a positive post-yielding stiffness and an increment of the maximum load at each cycle. The failure mode of BIEs is likely to be in most cases the same as for CCBs: low-cycle fatigue induced fracturing at the mid-length after the onset of local buckling. However, as the results of Skalomenos et al. [3] indicate, the introduction of the eccentricity can delay, in terms of imposed displacement or drift ratio, the onset of local buckling and subsequent fracture.

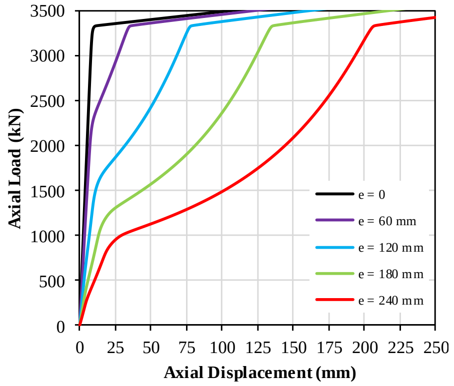

Fig. 3 – Influence of eccentricity in the tension force-displacement behaviour of 178×178×16 HSS BIEs

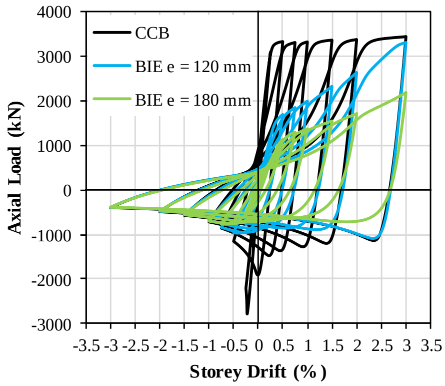

Fig. 4 – Axial force vs. storey drift for 178×178×16 HSS BIEs and CCBs under cyclic load

As can be inferred from the behaviour described in the preceding lines, the conventional force-based seismic design procedures of many modern design codes, such as the National Building Code of Canada [6], are not well-suited for use with BIEs. These procedures assume that the dissipating elements of the SFRS behave in an elastic-perfectly plastic manner, and, as such, can be sized by equating their yield strength to the expected seismic demands, scaled-down accounting for the system's ductility and overstrength. BIEs, however, present a response dissimilar to an elastic-perfectly plastic model and attain their maximum resistance at displacement levels that depend on the eccentricity and that might be too large to comply with serviceability limit states. Furthermore, the resistance they provide varies constantly with the imposed displacement, rendering the use of ductility-based seismic force reduction factors inappropriate. For these reasons, the authors propose a displacement-based procedure for the design of FIEBs, which is presented in detail in [4].

However, a displacement-based design procedure is ineffectual if the resulting structure is not able to attain the selected displacement levels. Thus, for their use in a displacement-based procedure, it is fundamental to be able to estimate what magnitude of displacement, or storey drift, a given BIE can safely sustain under cyclic loading, i.e. without being affected by local buckling, as it is the precursor of fracture.

3. Definition of parametric study and modelling considerations

With the objective of obtaining an empirical equation that would allow one to estimate a square HSS BIE's fracture life as a function of its global and local slenderness, and the eccentricity, a parametric study based on finite element model analyses in Abaqus [7] was undertaken. It was defined that the variables to consider would be the eccentricity to section height ratio, e/H, the global slenderness parameter, L/r, and the local slenderness ratio, b_{el}/t (H is the section's outside height, r its radius of gyration, t its wall thickness and b_{el} the width of the flat faces of the HSS, taken as $H - 4t$).

Given that the actual calibration of a fracture model requires extensive information which, for the moment, is not available for BIEs, the threshold of imminent failure is determined by the onset of plastic local buckling. The suitability of Abaqus to simulate local buckling has previously been established in the literature, e.g. [8].

The concept of the connections and *eccentering* assemblies considered in the development of the models is shown in Fig. 5. It is the same configuration considered for the design of buildings presented in [4]. It was selected accounting for its simplicity and cost-effectiveness, and also to produce the in-frame-plane bending of the BIE. It consists of a gusset- and knife- plate assembly, connected by bolted angles. The eccentricity is introduced by side plates that tie rigidly the HSS to the knife plate. Flare-bevel welds at the HSS's corners provide its connection to the side plates. The knife plate is detailed using a clearance with a length of twice the plate's thickness, t_g, to allow for the unrestrained rotation of the BIE's ends.

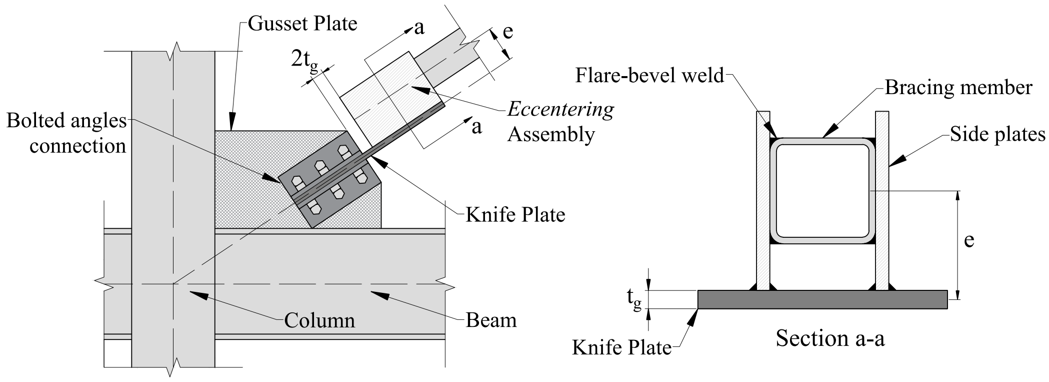

Fig. 5 – Example of the considered BIE to frame connection and *eccentering* assembly

In the numerical models, however, the bolted angles connection is not explicitly modelled, instead, a fixed end condition is enforced at the end of the knife plate clearance, as shown in Fig. 6. All plates and the HSS are modelled using shell elements (S4R) with 11 integration point through the thickness. The flare-bevel welds were modelled using solid elements to more realistically represent the interaction between the connected elements. The typical seed size of the shell elements varied from 2 mm to 6 mm as a function of the overall model's dimensions. Symmetry was used so that only a quarter of the actual BIE had to be modelled, reducing the computational expense. As is explained later, a model employing the same principles, but based on the published results in [3], was first constructed and analysed to validate the modelling considerations.

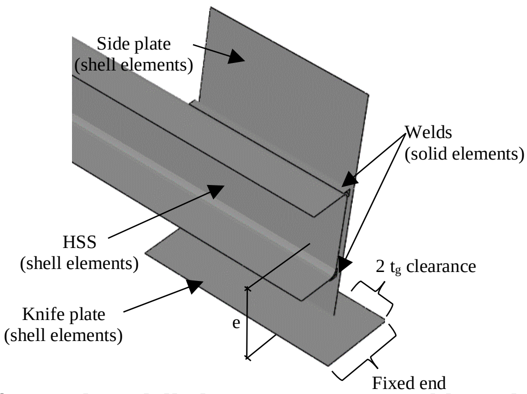

Fig. 6 – Detail of typical modelled *eccentering* assembly and connection

Table 1 presents the selected sections for the parametric study and the thickness of their side- (t_s) and knife-plates (t_g) and the length of the knife plate clearance (L_g). The thicknesses were defined so that the plates had sufficient strength to resist the maximum probable force that the HSS could develop in tension, i.e. $A_g R_Y F_Y$, with A_g being the gross area of the cross-section and $R_Y F_Y$ taken as 460 MPa, as per [9]. In all the models the hinge to hinge length was taken as 5470 mm, and both the side plated *eccentering* assembly's length and the knife plate's width were taken as 300 mm. These dimensions are within the expected range for a BIE in a 6 m by 4 m bay, considering the size of the columns, beams and gusset plate and bolted angle connections. Recognising that for all commercially available square HSS sections with the same outside height, the value of r is approximately constant, five groups of sections with constant height were selected to provide five approximate values for the L/r variable: 55, 80, 115, 150 and 200. Within each group, all six or five commercially available thicknesses were included in the study, as can be observed in Table 1. The Table also indicates whether the selected sections comply with the global and local slenderness limits of [9] for HSSs employed in CBFs (the global slenderness must be between 70 and 200). Finally, for each section, nine levels of e/H were considered: 0 (CCB), 0.25, 0.5, 0.75, 1, 1.25, 1.5, 1.75 and 2, for a total of 243 individual analyses.

Table 1 – Selected sections and model dimensions

Section	H (mm)	L/r	b_{el}/t	Limiting b_{el}/t (CSA S16-14)	Complies with slenderness limits?	t_s (mm)	t_g (mm)	L_g (mm)
254×254×16	254.0	56.9	12.0	17.8	No	32.0	76.0	152.0
254×254×13	254.0	56.0	16.0	17.8	No	51.0	64.0	128.0
254×254×9.5	254.0	55.2	22.7	17.8	No	38.0	51.0	102.0
254×254×8.0	254.0	54.8	27.9	17.8	No	32.0	38.0	76.0
254×254×6.4	254.0	54.2	36.0	17.8	No	25.0	32.0	64.0
178×178×16	177.8	84.3	7.2	17.8	Yes	38.0	51.0	102.0
178×178×13	177.8	82.3	10.0	17.8	Yes	32.0	44.0	88.0
178×178×9.5	177.8	80.4	14.7	17.8	Yes	25.0	32.0	64.0
178×178×8.0	177.8	79.5	18.4	17.8	No	22.0	32.0	64.0
178×178×6.4	177.8	78.6	24.0	17.8	No	16.0	22.0	44.0
178×178×4.8	177.8	77.8	33.2	17.8	No	13.0	19.0	38.0
127×127×13	127.0	119.7	6.0	18.7	Yes	22.0	32.0	64.0
127×127×9.5	127.0	115.6	9.3	18.5	Yes	16.0	22.0	44.0
127×127×8.0	127.0	114.0	12.0	18.4	Yes	16.0	22.0	44.0
127×127×6.4	127.0	112.1	16.0	18.4	Yes	13.0	16.0	32.0
127×127×4.8	127.0	110.3	22.6	18.3	No	10.0	13.0	26.0
102×102×13	101.6	155.0	4.0	20.4	Yes	16.0	22.0	44.0
102×102×9.5	101.6	148.2	6.7	20.1	Yes	13.0	19.0	38.0
102×102×8.0	101.6	145.5	8.8	20.0	Yes	13.0	16.0	32.0
102×102×6.4	101.6	142.4	12.0	19.8	Yes	10.0	13.0	26.0
102×102×4.8	101.6	139.5	17.3	19.7	Yes	8.0	10.0	20.0
102×102×3.2	101.6	136.8	27.9	19.5	No	6.0	8.0	16.0
76×76×9.5	76.2	206.4	4.0	22.6	No	10.0	13.0	26.0
76×76×8.0	76.2	201.1	5.6	22.6	No	8.0	10.0	20.0
76×76×6.4	76.2	195.4	8.0	22.4	Yes	8.0	10.0	20.0
76×76×4.8	76.2	189.9	11.9	22.1	Yes	5.0	8.0	16.0
76×76×3.2	76.2	184.8	20.0	21.9	Yes	5.0	5.0	10.0

All models were subjected to the same loading protocol, which consisted of cycles of imposed equivalent drift ratio of increasing magnitude: ± 0.1, ± 0.25, ± 0.5, ± 0.75, ± 1, ± 1.5, ±2, ± 3, ± 4 and ± 5 %, each imposed for two cycles, as shown in Fig. 7. This load protocol is the same used in the tests presented in [3], although in this case the cycles initiate with the loading in compression instead of tension.

Regarding the material properties, a true stress-true strain curve based on real coupon data (specimen HS 152 from reference [10]) from a square HSS, scaled so that its yield stress, F_Y, was equal to the probable yield strength of HSSs according to [9], $R_Y F_Y$ = 460 MPa, was input into the software. The selected true stress-true strain curve is presented in Fig. 8. A combined hardening model, considering both isotropic and kinematic hardening, computed by the software based on the stress-strain curve was employed. For the plates, an elastic-perfectly plastic material with F_Y = 385 MPa was employed. The welds were modelled as elastic. No residual stresses were considered.

Both global imperfection of the BIE and local imperfection of the HSS were included in the models. Examples of the global and local buckled shapes considered in the models are shown in Fig. 9 and Fig. 10, respectively. The global buckled shape was scaled so that the maximum initial imperfection at the center of the brace was equal to 1/500 times the hinge to hinge length, and the local buckled shape was scaled to produce a local change of 1 % on the initial minimum distance across opposite faces of the HSS.

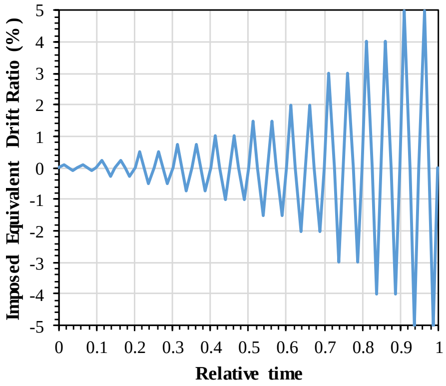

Fig. 7 – Loading protocol

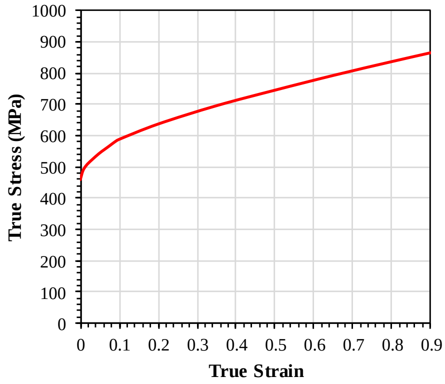

Fig. 8 – True stress-true strain curve for the HSS material (inelastic portion)

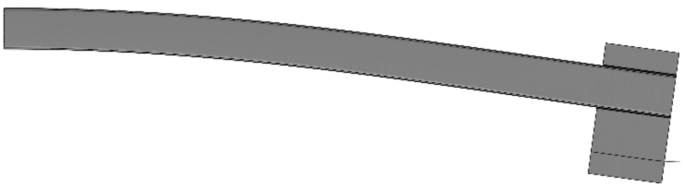

Fig. 9 – Example of deformed shape for global buckling imperfection

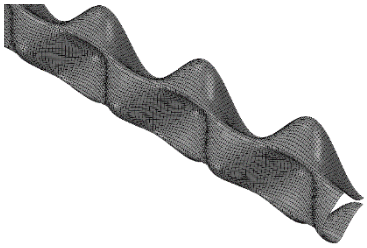

Fig. 10 – Example of deformed shape for local buckling imperfection

4. Validation of modelling approach

To verify the appropriateness of the modelling considerations described above, a model of one of the specimens tested by Skalomenos et al. [3], specimen G1-Oop-60, was constructed and analysed in Abaqus, using the information provided in [3]. Both the HSS and the gusset plate were modelled using shell elements, which was not possible for the *eccentering* assembly's elements due to their geometry. The initial imperfections were consistent with what is described in the previous section, and the material with the curve in Fig. 8., which was again scaled down to match the F_Y and F_U values reported in [3].

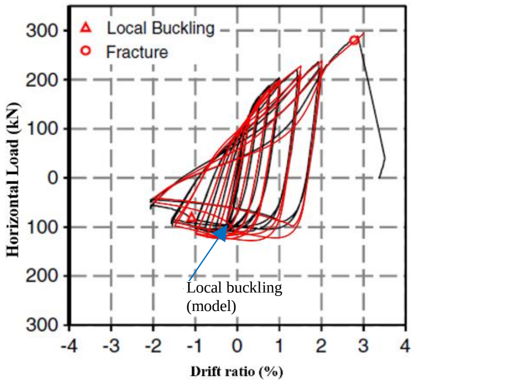

Fig. 11 – Comparison of results from Abaqus validation model with experimental results for specimen G1-Oop-60 from reference [3]

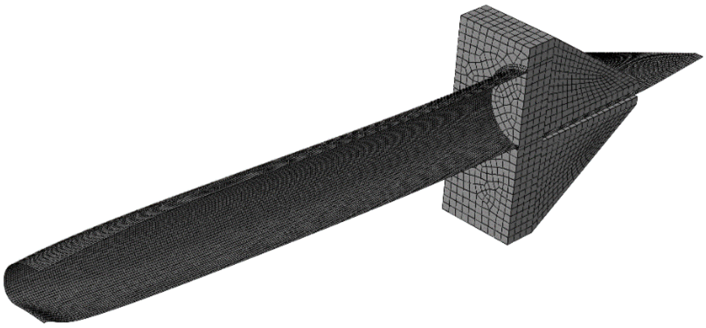

Fig. 12 – Abaqus validation model at onset of local buckling

Figure 11 presents the results from the so defined validation model, superimposed on the experimental force-drift hysteresis curve reported for specimen G1-Oop-60 in [3]. As can be noted, the proposed modelling approach produced a result that matches satisfactorily the experimental results, even though the actual stress-strain information for the materials involved was not available. The onset of local buckling was predicted within the same cycle as it occurred in the test, although slightly earlier. Figure 12 shows the deformed shape of the validation model at the onset of local buckling.

5 Results

For the 243 individual numerical analyses, force-drift hysteresis plots were obtained and the drift amplitude of the cycle in which the BIE developed local buckling, θ_{md}, was reported. As the precise occurrence of local buckling is not always evident in the hysteresis plots, it was identified by inspecting the animation of the deformation history of the models. 6 % was reported as the maximum drift ratio for the specimens for which local buckling was not observed, as the testing protocol had a maximum amplitude of 5 %. Figure 13 presents an example of the resulting force-drift hysteretic curve, including an indicator for the onset of local buckling. Figure 14 shows the deformed state of the same BIE's mid-length at the onset of local buckling.

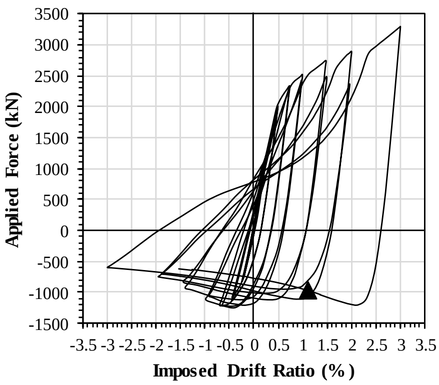

Fig. 13 – Example of obtained force – drift hysteretic curve for HSS 178×178×16 model with e/H=0.75, with indication for observed onset of local buckling

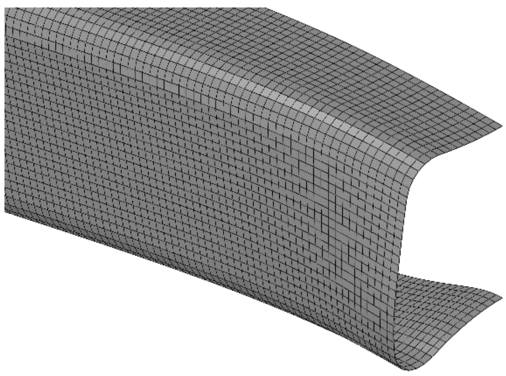

Fig. 14 – Incipient local buckling at mid length of HSS 178×178×16 model with e/H=0.75

The results show that, as expected, the fracture life increases with the eccentricity, with the section compactness and with the global slenderness. In the majority of cases, local buckling occurred at the expected location, but in some particular cases, such as for the 254×254×6.4 for e/H ratios larger than 1.5, it was observed that local buckling occurred in the top of the BIE toward the ends of the braces instead of at the bottom at the mid-length. This is presumably due to the formation of plastic hinges when the brace is loaded in tension, and this aspect will be further investigated at later stages of the research program, although preliminarily sections with such a large local slenderness do not seem to have much potential to be employed as BIEs. In Fig. 15 and Fig. 16, the observed maximum drift ratios for the HSS 102×102 and the HSS 178×178 models are presented. Note that according to these results, very compact sections would be able to sustain very large drift ratios without being affected by local buckling, and therefore be very well suited to be employed in FIEBs with large target deformation levels.

A non-dimensional combined slenderness parameter, $\lambda_0 = (L/r)/(b_{el}t)$ was defined to group together both slenderness parameters and analyse the relation of θ_{md} to λ_0 and e/H. Thus, it was possible, after eliminating outlier results, to obtain through multiple regression an expression that allows one to estimate the maximum allowable drift ratio as a function of the combined slenderness parameter and the eccentricity ratio. The obtained expression is given in Eq. (1). The so obtained regression model presents an adjusted R-square value of 0.98 and a root mean square error (RMSE) of 0.345. Figure 17 presents a scatter plot with the obtained point data, and the surface obtained with Eq. (1), Fig. 18 compares the observed values of θ_{md} with those resulting from the use of Eq. (1).

$$\theta_{md} = -0.4312 + 0.1943\lambda_0 + 0.6704e_0 - 0.001319\lambda_0^2 - 0.01833\lambda_0 e_0 + 0.241e_0^2 \quad (1)$$

It is recommended that when considered a given BIE for its use in a FIEB, its expected fracture life be estimated employing Eq. (1), considering a safety margin. Further research, however, including physical testing is required to obtain more information on the fracture life of BIEs and to further refine the proposed model.

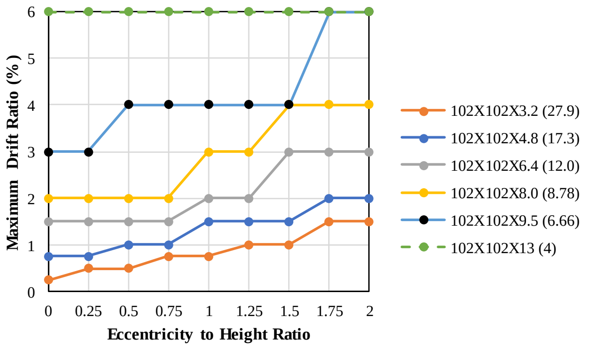

Fig. 15 – Observed maximum drift ratios for HSS 102×102 models (L/r ≈ 150)

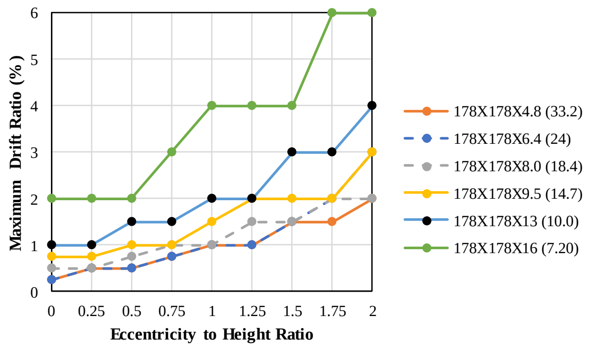

Fig. 16 – Observed maximum drift ratios for HSS 178×178 models (L/r ≈ 90)

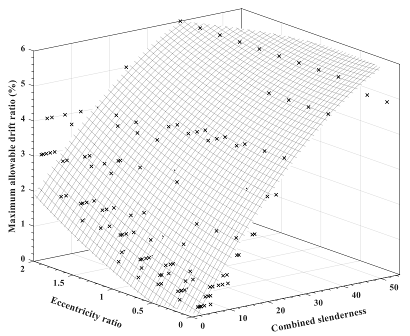

Fig. 17 – Maximum allowable drift ratio vs. combined slenderness and eccentricity ratio

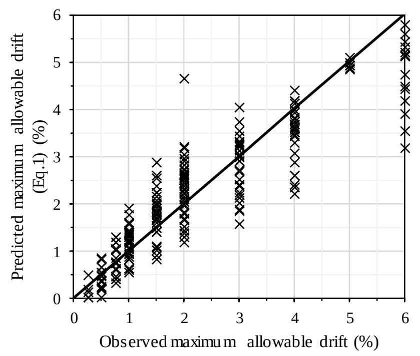

Fig. 18 – Maximum allowable drift ratios – observed vs. predicted by Eq. (1)

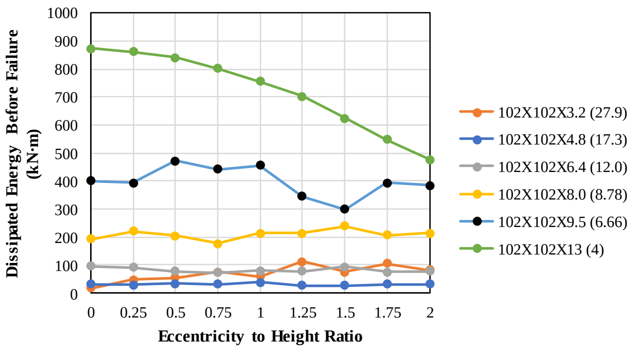

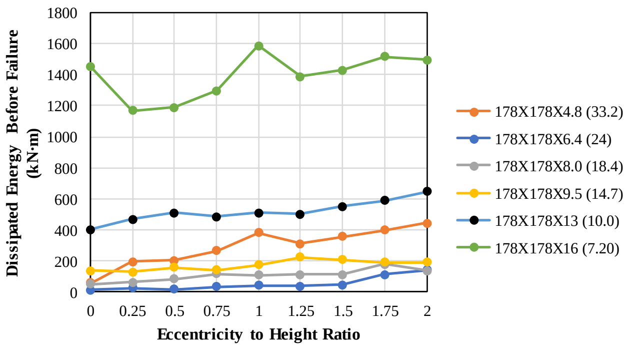

Fig. 19 – Dissipated energy prior to the onset of local buckling for HSS 102×102 models (L/r ≈ 150)

Fig. 20 – Dissipated energy prior to the onset of local buckling for HSS 178×178 models (L/r ≈ 90)

In addition to θ_{md}, the total dissipated energy by the BIEs before the onset of local buckling was also calculated. Figures 19 and 20, present the total energy dissipated by the HSS 102×102 and the HSS 178×178 models, as a function of the eccentricity. As can be observed, there is no clear correlation between the eccentricity and the energy dissipation capacity of the BIEs. Instead, the results suggest that the energy dissipation capacity is a property of the section itself. The downward trend of the curve for the HSS 102×102×13 model occurred because no local buckling was observed during the entire load protocol, therefore, because of the increasing eccentricity, the total amount of energy dissipated during the test decreased.

To obtain a better estimate of the actual damping that the BIEs would produce in a FIEB, the equivalent viscous damping ratio, ξ_{eq}, was calculated for each cycle based on its definition given in [11], using Eq. (2), where E_d is the energy dissipated during a complete cycle, F_m is the maximum force attained in the cycle and δ_m the displacement amplitude of the cycle.

$$\xi_{eq} = \frac{E_d}{2\pi F_m \delta_m} \tag{2}$$

The results of this calculation obtained for the Abaqus models of the HSS 178×178×16 are presented in Fig. 21 as an example. It can be noted that, for eccentricity ratios higher than 1.0, the maximum value of ξ_{eq} seems not to present much variation. However, it must be noted that neither the spacing of the cycle's amplitude nor the amount of data points that were registered in the analysis runs in Abaqus were fine enough to adequately obtain these results as, initially, it was not planned that the parametric study would be used to provide this information. For this reason, additional analyses were performed in OpenSees, with a higher resolution of data points and a finer increment of the displacement amplitude (cycles were defined in increments of 0.25 % equivalent drift ratio), in order to obtain more reliable information regarding the equivalent damping ratio of BIEs.

The results of these second set of analyses showed that although the maximum value of the equivalent damping ratio shows very little variation for a given section as a function of the eccentricity ratio, the displacement at which this maximum value of ξ_{eq} is attained did show a correlation with the eccentricity ratio. However, by having ξ_{eq} expressed instead as a function of the ductility demand, calculated with respect to the displacement of the first yield point obtained from tests under monotonic load, it was found that for BIEs with eccentricity ratios larger than 0.8, the maximum value for ξ_{eq} and the associated ductility demand are approximately constant. An example of these results is shown in Fig. 22 for BIEs of HSS 152×152×13.

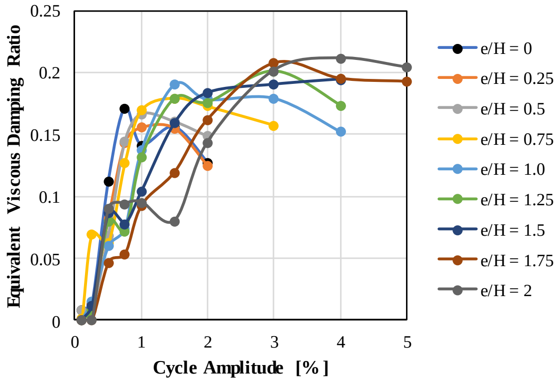

Fig. 21 – Equivalent viscous damping vs. cycle amplitude from Abaqus models for HSS 178×178×16

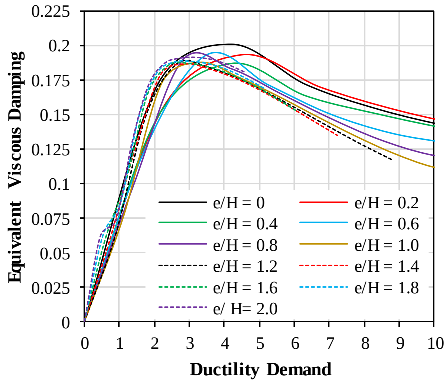

Fig. 22 – Equivalent viscous damping vs. ductility demand from OpenSees models for HSS 152×152×13

A formal model to estimate the values of ξ_{eq} of BIEs to be used in displacement-based design is yet to be developed. The values obtained in this research provide only an estimate of those, as actual values employable for design would require further calibration to ensure that they would provide adequate results under the effects of actual ground motions. The formal creation of these models was not considered in the scope of this research. However, considering that the maximum value of ξ_{eq} as a function of the ductility demand, μ, is nearly constant for a given section, and that it is not affected by the eccentricity, the use on BIEs of the models developed by Wijesundara et al. [12] for the equivalent damping of CCBs, given by Eq. (3), is considered appropriate in the interim. Their use as part of the design procedure developed by the authors [4] has so far yielded acceptable results.

$$\begin{aligned} \mu \leq 2: \quad & \xi_{eq} = 0.03 + \left(0.23 - \frac{\lambda}{15}\right)(\mu - 1) \\ \mu > 2: \quad & \xi_{eq} = 0.03 + \left(0.23 - \frac{\lambda}{15}\right) \\ & \lambda = \frac{L}{r}\sqrt{\frac{F_Y}{\pi^2 E}} \end{aligned} \tag{3}$$

5. Conclusions

BIEs appear as innovative dissipative elements whose use in seismic-force-resisting systems has the potential to overcome some of the major shortcomings of conventional concentric braces, specifically those related to their invariably high stiffness and their propensity to premature failure due to low-cycle fatigue fracture, as the introduction of the eccentricity is expected to delay the onset of local buckling. However, due to their particular force-deformation behaviour they are better suited to displacement-based design procedures instead of force-based ones. For this reason, it is of great relevance to estimate the displacement level that a given BIE would be able to sustain safely under cyclic loading.

With the intent of doing so, a numeric parametric study was undertaken for square HSSs, treating the eccentricity ratio, the global slenderness ratio and the local slenderness ratio as variables. As expected, the results showed that the fracture life increases with the eccentricity ratio, the section compactness, and overall slenderness. Using the results from the 243 individual analyses, a prediction equation based on multiple regression was obtained to estimate the maximum allowable drift ratio for BIEs as a function of the eccentricity ratio and a combined slenderness parameter that encompasses both local and global slenderness. Through a validation model that approximated well the experimental results presented by Skalomenos et al. in their seminal paper on BIEs [3], it was verified that the modelling approach used in the parametric study was able to simulate the response of BIEs, in particular the onset of local buckling.

Additionally, information was gathered regarding the energy dissipation capacity of BIEs and the equivalent damping ratio associated with it. It was found that the net energy dissipation capacity previous to the onset of local buckling does not depend on the eccentricity; it seems instead to be a function of the geometry of the bracing member and its material. As well, it was determined that neither the maximum equivalent damping ratio nor the ductility demand at which it occurs for a given BIE depend on the eccentricity. Thus, until properly calibrated methods specifically for BIEs are presented, it is suggested that the relations developed by Wijesundara et al. for estimating the equivalent damping ratio of concentric braces be used to approximate the equivalent damping ratio of BIEs in a displacement-based design scenario.

All the results presented herein are to be considered as preliminary, given that so far, no test results have been published for BIEs made of square HSSs or employing the *eccentering* assembly here considered. Further stages of the ongoing research program include the physical testing of BIEs such as those considered in this study. The data obtained will shed additional light on the actual behaviour and failure mode of BIEs and will be used to validate, refine or refute the proposed model.

6. Acknowledgements

The authors would like to thank DPHV Structural Consultants, ADF Group Inc. and Constructions Proco for their generous technical and financial support, as well as the Natural Sciences and Engineering Research Council (NSERC) of Canada, the Fonds de Recherche du Québec – Nature et Technologies (FRQ-NT) and the Centre d'Études Interuniversitaire des Structures sous Charges Extrêmes (CEISCE). The first author also wishes to acknowledge Universidad de Costa Rica for financing the undertaking of his doctoral studies.

7. References

[1] Tang X, Goel S (1989): Brace fractures and analysis of phase I structure. *ASCE Journal of Structural Engineering*, **115**(8), 1960-1976.

[2] Tremblay R (2002): Inelastic response of steel bracing members. *Journal of Steel Constructional Steel Research*, **58**(5-8), 665-701

[3] Skalomenos K, Inamasu H, Shimada H, Nakashima M (2017): Development of a steel brace with intentional eccentricity and experimental validation. *ASCE Journal of Structural Engineering*, DOI: 10.1061/(ASCE)ST.1943-541X.0001809

[4] González Ureña A, Tremblay R, Rogers CA (2020): Design and performance of frames with intentionally eccentric braces. *17th World Conference on Earthquake Engineering*, Sendai, Japan. Paper nº C000830 (Submitted)

[5] McKenna F, Fenves G, Scott M (2004): *Open system for earthquake engineering simulation*. Pacific Earthquake Engineering Center, University of California, Berkeley, USA

[6] NRCC (2015): *National building code of Canada 2015, 14th ed*. National Research Council of Canada, Ottawa, Canada

[7] Dassault Systèmes (2018): *Abaqus/CAE 2019*. Dassault Systèmes Simulia Corp. Providence, USA

[8] Fell B, Kanvinde A, Deierlein G (2010): *Large-scale testing and simulation of earthquake induced ultra low cycle fatigue in bracing members subjected to cyclic inlelastic buckling.* The John A. Blume Earthquake Engineering Center, Stanford University, Stanford, USA

[9] CSA (2014): *CSA S16-14: Design of steel structures.* Canadian Standards Association, Toronto, Canada

[10] Moreau R (2014): *Evaluation of the "Modified-Hidden-Gap" connection for square HSS Brace Members.* Master`s thesis, McGill University, Montréal, Canada

[11] Chopra AK (2012): *Dynamics of structures, 4th edition*, Prentice Hall, Upper Saddle River, NJ, USA

[12] Wijesundara K, Nascimbene R, Sulivan T (2011): Equivalent viscous damping for steel concentrically braced frame structures. *Bull. Earthquake Eng.* **9**, 1535-1558

